Journal of Imaging Science and Technology® 66(2): 020401-1–020401-10, 2022.

Coupling Modeling and Analysis of the Tension System for Roll-to-Roll Gravure Printing Machines

Ziyu Wang and Shanhui Liu
Faculty of Printing, Packaging Engineering and Digital Media Technology, Xi'an University of Technology, Shaanxi, China
E-mail: shanhuiliu@xaut.edu.cn

Lei Feng
Shaanxi Beiren Printing Machinery Co., Ltd., Shaanxi, China

Zengqiang Zhang and Jiaqi Liu
Faculty of Printing, Packaging Engineering and Digital Media Technology, Xi'an University of Technology, Shaanxi, China

Abstract. *Control accuracy of tension system is an important index in roll-to-roll gravure printing machines. However, the complex relationships of the tension system make the problem of coupling model difficult to be solved, which has limited the improvement of tension control accuracy. Therefore, a coupling mechanism model of global tension system is established and analyzed for the gravure printing machines in this study. According to the working principles and assumptions, tension model of the two-roller system is derived by considering the effects of drying temperature, and then the tension models of subsystem including unwinding subsystem, printing subsystem and rewinding subsystem are established. Based on these, the global coupling mechanism model of the tension system is established for roll-to-roll gravure printing machines. Finally, the coupling model is analyzed by MATLAB simulation, and the simulation results show that the tension system model established in this paper can accurately reflect the characteristics of tension system.*
[DOI: 10.2352/J.ImagingSci.Technol.2022.66.2.020401]

1. INTRODUCTION

Roll-to-roll gravure printing machine has the advantages of continuous production, thick ink layer and stable process. It is widely used in traditional packaging printing and is considered one of the highest throughput printed electronic equipment for manufacturing disposable and flexible electronic devices on flexible substrates at a low cost. Tension system is the most important part of the control system in roll-to-roll gravure printing machines. In the process of printing, the substrate must pass through each unit sequentially under the condition of stable tension. If the tension control accuracy is insufficient, the register accuracy will be greatly reduced, and even the substrate will be broken. Therefore, high precision tension control is the premise and foundation of high-quality printing. But it is very difficult to control the tension system of the gravure printing machine because of the characteristics of the tension system including nonlinear, strong coupling and strong disturbance. The accurate model of the tension system is the basis of designing high precision tension controller. Unfortunately, the current tension system model cannot accurately reflect the global coupling relationships of the tension system, and the mechanism of the tension fluctuation caused by multi-source interference including temperature variation remains to be investigated. Hence, it is imperative to scrutinize the mathematical model which can reflect the global coupling relations of multi-physical quantities for the gravure printing machine.

In recent years, many scholars have done excellent work in the modeling of tension systems for roll-to-roll machines. Jiang [1] and Liu [2] studied the modeling and controller of unwinding tension system. Jeon established linear dancer system model of drying process for the two-roller unit [3]. Dwivedul analyzed effect of backlash on web tension in roll-to-roll manufacturing systems [4]. Jeong analyzed the factors causing the tension fluctuation in the roll-to-roll system and established a mathematical model for the tension system [5]. Seki modeled and analyzed the effects of viscoelasticity on the tension of roll-to-roll systems [6]. Huang analyzed the coil tension of core transformer and established the tension model of unwinding system and rewinding system [7]. Gu designed a rod spring mechanism to measure tension and established a mathematical model of the mechanism [8]. He established the tension model of the influence of roller eccentricity on web tension and the periodic disturbance [9]. Seshadri described modeling and control of a rotating turret winder in the rewinding section [10]. Wang studied the causes of the fluctuation of unwinding tension system [11]. Based on the dynamic models of web winding system, Chen designed a robust decentralized $H\infty$ control method [12]. Kuznetsov analyzed the uncertainty disturbance randomness of the rewinding system parameters and established mathematical models of cable winding machine [13]. Torres [14, 15] and He [16] analyzed the mechanism of temperature induced variation of substrate tension and improved the tension system model. Lee analyzed the influence of elasticity and thermal deformation of substrate in the production of printed electronic devices [17].

Received June 24, 2021; accepted for publication Sept. 19, 2021; published online Oct. 27, 2021. Associate Editor: Zhuangzhi Ye.
1062-3701/2022/66(2)/020401/10/$25.00

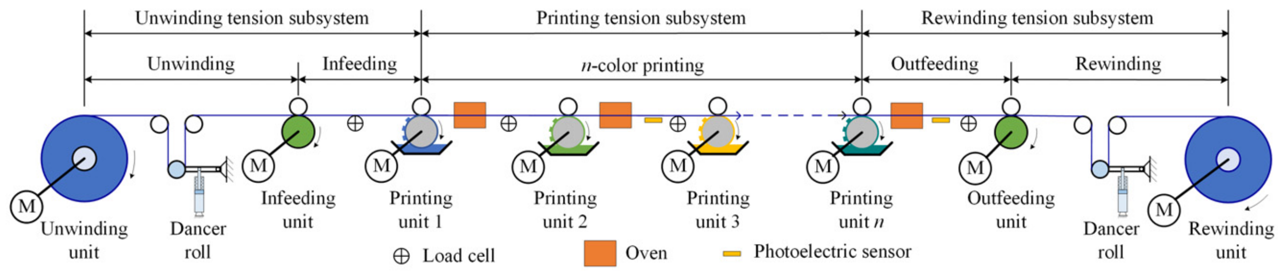

Figure 1. Schematic diagram of a roll-to-roll *n*-color gravure printing machine.

Most of the research on the tension system modeling focuses on the local modeling of a certain tension subsystem, and few of the research on the global coupling modeling of the roll-to-roll gravure machine. Therefore, the aim of this research is to establish a coupling mechanism model of global tension system for the gravure printing machines. This paper is structured as follows: Section 2 analyzes the structure of the global tension system of roll-to-roll gravure printing machine. Section 3 establishes a coupling model of the global tension system. Section 4 analyzes and verifies the coupling model of four-color gravure printing machine by simulation.

2. ANALYSIS OF GLOBAL TENSION SYSTEM

Roll-to-roll gravure printing machine is a typical complex electromechanical integration system, which involves many subjects such as machinery, electrical, material, friction, heat transfer, control, etc. The typical schematic diagram of a roll-to-roll n-color gravure printing machine is presented in Figure 1, and n stands for the total number of printing units. The gravure printing machine is composed of an unwinding unit, an infeeding unit, multiple printing units, an outfeeding unit and a rewinding unit, and n stands for the total number of printing units. In the machines, all of the driving shafts are driven by independent servo motors.

During the printing process, the substrate passes through each unit sequentially under a certain tension. For example, the tension fluctuation of substrate is usually less than 2% in printed electronic devices. The global tension system is composed of three tension subsystems: unwinding tension subsystem, printing tension subsystem and rewinding tension subsystem. The unwinding tension subsystem consists of the unwinding unit and the infeeding unit. The printing tension subsystem includes printing unit 1 to printing unit n. The rewinding unit and the outfeeding unit constitute the unwinding tension subsystem. Two dancer rollers are used to measure the tension signals and reduce tension fluctuations simultaneously in the unwinding and rewinding units. Load cells are installed at idle rollers in the middle of continuous process for tension pickup.

The unwinding unit is the starting part of substrate tension, which is produced and transferred to subsequent functional unit step by step. In the process of unwinding and rewinding, the diameter and rotational inertia of the unwinding roller and rewinding roller vary with time, which makes tension system into a time-variant and nonlinear system. Angular velocity of the printing unit 1 is benchmark velocity of the whole tension system, and angular velocity of other units is adjusted according to substrate tension measured by load cells or dancer rollers. It can be seen from Fig. 1 that the velocity adjustment of each unit motor from infeeding unit to outfeeding unit affects both the substrate tension of current unit and the substrate tension of next unit. Substrate tension output of each unit is also used as the input of the next tension unit, which affects the tension output of the latter tension unit. Therefore, the tension system is a strong coupling system in roll-to-roll gravure printing machines. In addition to these, substrate tension is also affected by many factors such as drying temperature, roller's dynamic characteristics, correction and reversing movement, etc.

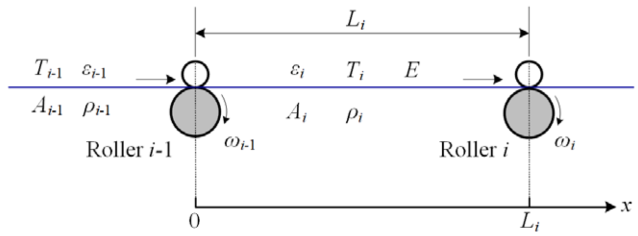

Figure 2. Structure of two-roller system.

3. COUPLING MODELING OF GLOBAL TENSION SYSTEM

The global tension system is comprised of several tension subsystems in the roll-to-roll gravure printing machine. Hence, we first establish the mathematical model of tension subsystems, and then, the tension model of each subsystem is integrated to complete the coupling model of the global tension system.

3.1 *Tension Model of Two-Roller System*

The structure of two-roller system is shown in Figure 2. Where T_{i-1} and T_i are substrate tension, ε_{i-1} and ε_i are substrate strain, ρ_{i-1} and ρ_i are the material densitiy of the substrate, E is Young's modulus of substrate, L_i is the length of the substrate, ω_{i-1} and ω_i are the angular velocity of two rollers.

It is assumed that there is no slippage between web material and rollers and no mass transfer between the substrate material and the environment. According to the mass conservation law, the mass change of the substrate between two rollers is equal to the difference between the incoming substrate mass and the outflow substrate mass in unit time. Thus, the following equation can be obtained:

$$\begin{aligned}\frac{d}{dt}\left[\int_0^{L_i(t)} \rho_i(x,t)A_i(x,t)\,dx\right] &= \rho_{i-1}(0,t)A_{i-1}(t)\omega_{i-1}(t)R_{i-1}(t)\\ &\quad - \rho_i(L_i,t)A_i(t)\omega_i(t)R_i(t).\end{aligned} \tag{1}$$

Where R_i is the roller radius, A_i is the cross-sectional area of substrate, x implies the substrate position in substrate proceeding direction.

From the definition of strain, the relation between the stretched and the unstretched length of the substrate element can be written as follows:

$$\frac{\rho_i(x,t)A_i(x,t)}{\rho_{ui}(x,t)A_{ui}(x,t)} = \frac{1}{1+\varepsilon_i(x,t)}. \tag{2}$$

Where u means the unstretched state of the substrate. Then Eq. (1) can be written as:

$$\begin{aligned}\frac{\mathrm{d}}{\mathrm{d}t}\left[\int_0^{L_i(t)} \frac{\rho_{ui}(x,t)A_{ui}(x,t)}{1+\varepsilon_i(x,t)}\,\mathrm{d}x\right] &= \frac{\rho_{u(i-1)}(0,t)A_{u(i-1)}(t)\omega_{i-1}(t)R_{i-1}(t)}{1+\varepsilon_{i-1}(t)}\\ &\quad - \frac{\rho_{ui}(L_i,t)A_{ui}(t)\omega_i(t)R_i(t)}{1+\varepsilon_i(t)}.\end{aligned} \tag{3}$$

It is assumed that the cross-sectional area of the substrate in unstretched state does not vary along the substrate, and the density and the Young's modulus of the substrate in the unstretched state are constant over the cross-section. We can obtain:

$$\begin{aligned}\rho_{ui}(x,t)A_{ui}(x,t) &= \rho_{ui}(L_i,t)A_{ui}(t)\\ &= \rho_{u(i-1)}(0,t)A_{u(i-1)}(t).\end{aligned} \tag{4}$$

So Eq. (3) can be rewritten as:

$$\frac{\mathrm{d}}{\mathrm{d}t}\left[\int_0^{L_i(t)} \frac{1}{1+\varepsilon_i(x,t)}\,\mathrm{d}x\right] = \frac{\omega_{i-1}(t)R_{i-1}(t)}{1+\varepsilon_{i-1}(t)} - \frac{\omega_i(t)R_i(t)}{1+\varepsilon_i(t)}. \tag{5}$$

It is assumed that the strain of the substrate does not change within the substrate span. We can rewrite Eq. (5) as follows:

$$\frac{\mathrm{d}}{\mathrm{d}t}\left[\frac{L_i(t)}{1+\varepsilon_i(t)}\right] = \frac{\omega_{i-1}(t)R_{i-1}(t)}{1+\varepsilon_{i-1}(t)} - \frac{\omega_i(t)R_i(t)}{1+\varepsilon_i(t)}. \tag{6}$$

Generally, $\varepsilon \ll 1$, so Eq. (6) can be written:

$$\begin{aligned}&\frac{\mathrm{d}L_i(t)}{\mathrm{d}t}[1-\varepsilon_i(t)] - L_i(t)\frac{\mathrm{d}\varepsilon_i(t)}{\mathrm{d}t}\\ &= \omega_{i-1}(t)R_{i-1}(t) - \omega_i(t)R_i(t)\\ &\quad - \omega_{i-1}(t)R_{i-1}(t)\varepsilon_{i-1}(t) + \omega_i(t)R_i(t)\varepsilon_i(t).\end{aligned} \tag{7}$$

According to the Hooke's law $T = AE\varepsilon$, Eq. (7) can be further written as:

$$\begin{aligned}L_i(t)\frac{\mathrm{d}T_i(t)}{\mathrm{d}t} &= [AE - T_i(t)]\omega_i(t)R_i(t)\\ &\quad - [AE - T_{i-1}(t)]\omega_{i-1}(t)R_{i-1}(t)\\ &\quad + [AE - T_i(t)]\frac{\mathrm{d}L_i(t)}{\mathrm{d}t}.\end{aligned} \tag{8}$$

Formula (8) is the tension model of two-roller system and reveals the multi-source mechanism of substrate tension variation. It can be seen from the mathematical model that the system has nonlinear characteristics.

If L_i is a constant value, that is, the span length of substrate between roller $i-1$ and roller i is unchanged, Eq. (8) can be written as follows:

$$\begin{aligned}L_i\frac{\mathrm{d}T_i(t)}{\mathrm{d}t} &= [AE - T_i(t)]\omega_i(t)R_i(t)\\ &\quad - [AE - T_{i-1}(t)]\omega_{i-1}(t)R_{i-1}(t).\end{aligned} \tag{9}$$

The Figure 3 shows the schematic diagram of the two-color printing system. Where ε_{D_i} is the substrate strain inside the oven, and L_{D_i} is the substrate length in the oven, t_D is the drying temperature of the oven, t_E is the ambient temperature outside the oven, a is the position where the substrate enters the oven, b is the position where the substrate is brought out of the oven.

Because the heating and drying time of the substrate after entering the oven is very short, it can be considered that the substrate temperature in the oven is equal to the drying temperature, and the substrate temperature outside the oven is equal to the ambient temperature. It is assumed that the substrate strain is equal at the same temperature, and the length of the substrate inside and outside the oven remains unchanged. As shown in Fig. 3, the substrate span between two printing rollers can be divided into three parts according to the temperature distribution. We can obtain:

$$\begin{aligned}\int_0^{L_i} \frac{1}{1+\varepsilon_i(x,t)}\,\mathrm{d}x &= \int_0^{a} \frac{1}{1+\varepsilon_i(x,t)}\,\mathrm{d}x\\ &\quad + \int_a^{b} \frac{1}{1+\varepsilon_{Di}(x,t)}\,\mathrm{d}x\\ &\quad + \int_b^{L_i} \frac{1}{1+\varepsilon_i(x,t)}\,\mathrm{d}x.\end{aligned} \tag{10}$$

Because the strain of the substrate remains constant within the substrate span, we calculate the integral part as follows:

$$\int_0^{L_i} \frac{1}{1+\varepsilon_i(x,t)}\,\mathrm{d}x = \frac{L_i - L_{Di}}{1+\varepsilon_i(t)} + \frac{L_{Di}}{1+\varepsilon_{Di}(t)}. \tag{11}$$

Combining the Eqs. (6) and (11), we can obtain:

$$\begin{aligned}\frac{\mathrm{d}}{\mathrm{d}t}\left[\frac{L_i - L_{Di}}{1+\varepsilon_i(t)} + \frac{L_{Di}}{1+\varepsilon_{Di}(t)}\right] &= \frac{\omega_{i-1}(t)R_{i-1}(t)}{1+\varepsilon_{i-1}(t)}\\ &\quad - \frac{\omega_i(t)R_i(t)}{1+\varepsilon_i(t)}.\end{aligned} \tag{12}$$

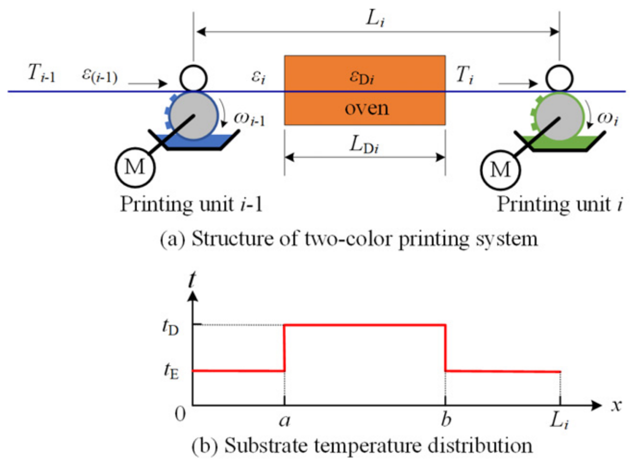

Figure 3. Schematic diagram of two-color printing system.

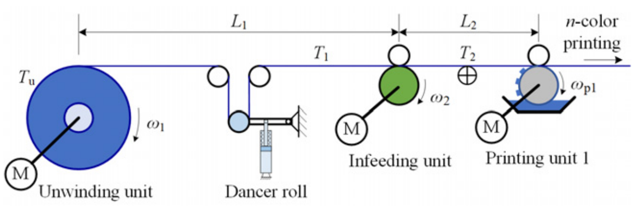

Figure 4. Structure of the unwinding subsystem.

Referring to the previous derivation, we can obtain the tension model of the two-color printing system as follows:

$$\left[L_i + L_{Di}\left(\frac{E}{E_{Di}} - 1\right)\right]\frac{\mathrm{d}T_i(t)}{\mathrm{d}t} = [AE - T_i(t)]\omega_i(t)R_i(t) - [AE - T_{i-1}(t)]\omega_{i-1}(t)R_{i-1}(t). \tag{13}$$

The multi-source mechanism of substrate tension variation is reflected in two-color printing system by Eq. (13).

3.2 *Tension Model of the Unwinding Subsystem*

The unwinding subsystem comprises an unwinding unit and an infeeding unit, the structure of which is shown in Figure 4. Where L_1 is the substrate length of the unwinding section, L_2 is the substrate length of the infeeding section, T_u is the residual tension in the unwinding roll, T_1 is the substrate tension of the unwinding section, T_2 is the substrate tension of the infeeding section, and ω_1, ω_2 and ω_{p1} are the angular velocity of the unwinding roll, infeeding roll and printing unit 1, respectively. The function of the unwinding system is to expand substrate according to the printing production requirements, and gradually transfer it to the subsequent units. The stability of this part of tension is the basis of the operation for the whole system.

As shown in Figure 5, the radius of the unwinding roll decreases with the unwinding process, which makes the substrate length of the unwinding unit change at the same time. Where R_1 is the radius of the unwinding roll, r is the radius of the first guide roller in the dancer roll, L_{A1} is the center distance between the unwinding roll and the first guide roller, L_{u1} is the substrate length between the unwinding unit and the first guide roller.

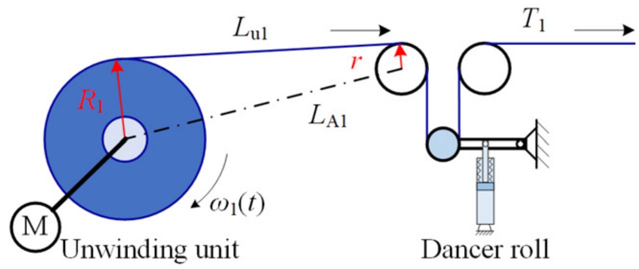

Figure 5. Structure of the unwinding unit.

According to the geometric relationship, L_{u1} can be calculated as follows:

$$L_{u1}(t) = \sqrt{L_{A1}^2 - [R_1(t) - r]^2}. \tag{14}$$

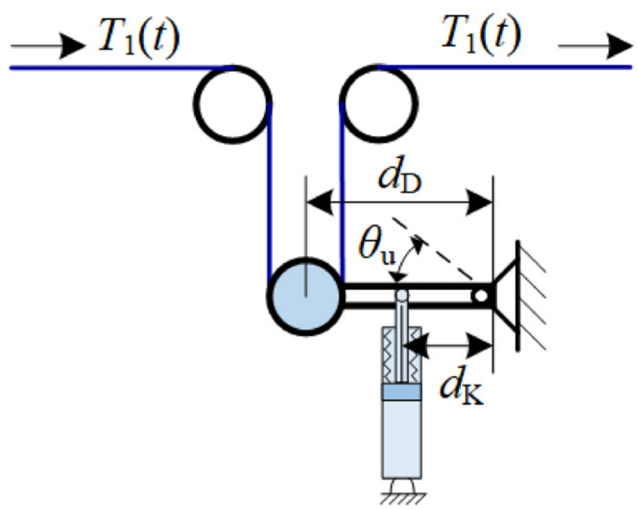

Figure 6. Structure of the dancer roll.

The structure of the dancer roll is shown in Figure 6. Where d_D is the length of the dancer arm, θ_u is the deflection angle of the dancer arm in the unwinding unit, d_K is the distance between the cylinder and the center of the rotation of the dancer arm. Because θ_u changes very little in the unwinding process, the length of the substrate in the dancer roll can be calculated as follows:

$$L_D(t) = L_0 - 2d_D\theta_u(t). \tag{15}$$

Where L_D is the substrate length in the dancer roll, L_0 is the substrate length in the dancer roll when the tension is in equilibrium.

Combining Eqs. (14) and (15), the calculation method of substrate length $L_1(t)$ can be obtained as follows:

$$L_1(t) = L_{u1} + \sqrt{L_{A1}^2 - [R_1(t) - r]^2} - 2d_D\theta_u(t). \tag{16}$$

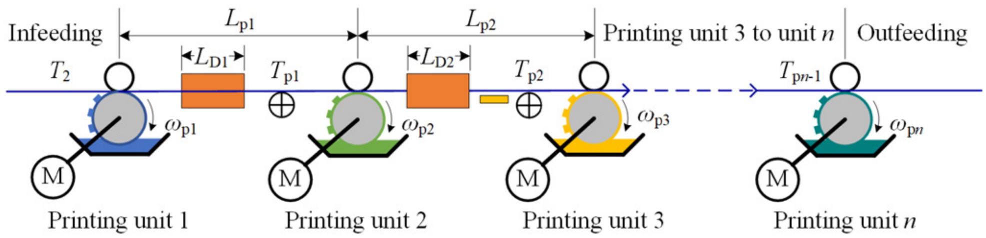

Figure 7. Structure of the n-color printing subsystem.

Where L_{u1} is the substrate length from the first guide roll to the infeeding roll when substrate tension is stable in the dancer roll.

We ignore the friction between substrate and rollers and the friction of the rotating part in the dancer roll. According to the principle of torque balance, the tension model of the dancer roll can be obtained as follows:

$$\begin{cases} T_1(t) = -\dfrac{1}{2d_D}\left[J_D\dfrac{\mathrm{d}^2\theta_u(t)}{\mathrm{d}t^2} + B\dfrac{\mathrm{d}\theta_u(t)}{\mathrm{d}t} - F_u(t)d_K\right] \\ F_u(t) = P_u(t)A_C - K\theta_u(t)\, d_{\mathrm{K}}. \end{cases} \tag{17}$$

Where J_D is the equivalent inertia of the dancer roll, B is the damping coefficient of the pendulum shaft, F_u is the thrust of the cylinder, P_u is the working pressure of the cylinder, A_C is the piston area of the cylinder, K is elastic coefficient of the spring in the cylinder.

As shown in Fig. 4, the unwinding subsystem can be regarded as the series of two two-roller systems. We ignore the influences of manufacturing errors, assembly errors and other factors, so L_2, R_2 and R_{p1} are fixed values. Combining with Eqs. (8) and (9), the tension model of the unwinding subsystem can be obtained:

$$\begin{cases} L_1(t)\dfrac{\mathrm{d}T_1(t)}{\mathrm{d}t} = [AE - T_1(t)]R_2\omega_2(t) \\ \qquad - [AE - T_u]R_1(t)\omega_1(t) \\ \qquad + [AE - T_1(t)]\dfrac{\mathrm{d}L_1(t)}{\mathrm{d}t} \\ L_2\dfrac{\mathrm{d}T_2(t)}{\mathrm{d}t} = [AE - T_2(t)]R_{p1}\omega_{p1}(t) \\ \qquad - [AE - T_1(t)]R_2\omega_2(t). \end{cases} \tag{18}$$

According to Eqs. (16) and (17), we can obtain the auxiliary equation of the tension model of the unwinding subsystem as follows:

$$\begin{cases} L_1(t) = L_{u1} + \sqrt{L_{A1}^2 - [R_1(t) - r]^2} - 2d_D\theta_u(t) \\ T_1(t) = -\dfrac{1}{2d_D}\left[J_D\dfrac{\mathrm{d}^2\theta_u(t)}{\mathrm{d}t^2} + B\dfrac{\mathrm{d}\theta_u(t)}{\mathrm{d}t} - F_u(t)\, d_K\right] \\ F_u(t) = P_u(t)A_C - K\theta_u(t)\, d_K. \end{cases} \tag{19}$$

3.3 *Tension Model of the Printing Subsystem*

The n-color printing subsystem is consisted of n printing units, the structure of which is shown in Figure 7. Where T_{p_i} is the substrate tension of the printing section i, L_{p_i} is the substrate length of the printing section i, L_{D_i} is the substrate length of the printing section i in the oven, ω_{p_i} is the angular velocity of the printing unit i. In addition, R_{p_i} is the radius of the printing roll i. The printing subsystem can be regarded as the series of $n-1$ two-color printing system.

It is assumed that the manufacturing errors and the assembly errors are equal to zero, so L_{p_i}, L_{D_i} and R_{p_i} are fixed values. Combining with Eq. (13) and the relationship between adjacent printing units, the tension model of the n-color printing subsystem can be obtained as follows:

$$\begin{cases} \left[L_{p1} + L_{D1}\left(\dfrac{E}{E_{D1}} - 1\right)\right]\dfrac{\mathrm{d}T_{p1}(t)}{\mathrm{d}t} \\ \quad = [AE - T_{p1}(t)]R_{p2}\omega_{p2}(t) \\ \qquad - [AE - T_2(t)]R_{p1}\omega_{p1}(t) \\ \left[L_{p2} + L_{D2}\left(\dfrac{E}{E_{D2}} - 1\right)\right]\dfrac{\mathrm{d}T_{p2}(t)}{\mathrm{d}t} \\ \quad = [AE - T_{p2}(t)]R_{p3}\omega_{p3}(t) \\ \qquad - [AE - T_{p1}(t)]R_{p2}\omega_{p2}(t) \\ \vdots \\ \left[L_{p(n-1)} + L_{D(n-1)}\left[\dfrac{E}{E_{D(n-1)}} - 1\right]\right]\dfrac{\mathrm{d}T_{p(n-1)}(t)}{\mathrm{d}t} \\ \quad = [AE - T_{p(n-1)}(t)]R_{pn}\omega_{pn}(t) \\ \qquad - [AE - T_{p(n-2)}(t)]R_{p(n-1)}\omega_{p(n-1)}(t). \end{cases} \tag{20}$$

It can be seen from (20) that the tension model of the n-color printing subsystem is consisted of $n-1$ tension models of the two-color printing system which are coupled with each other.

3.4 *Tension Model of the Rewinding Subsystem*

The rewinding tension subsystem consists of an outfeeding unit and a rewinding unit, the structure of which is shown in Figure 8. Where L_3 is the substrate length of the outfeeding section, L_4 is the substrate length of the rewinding section, T_3 is the substrate tension of the outfeeding section, T_4 is the substrate tension of the rewinding section, R_4 is the radius of the rewinding roll, ω_{pn}, ω_3 and ω_4 are the angular velocity of the printing unit n, outfeeding roll, rewinding roll,

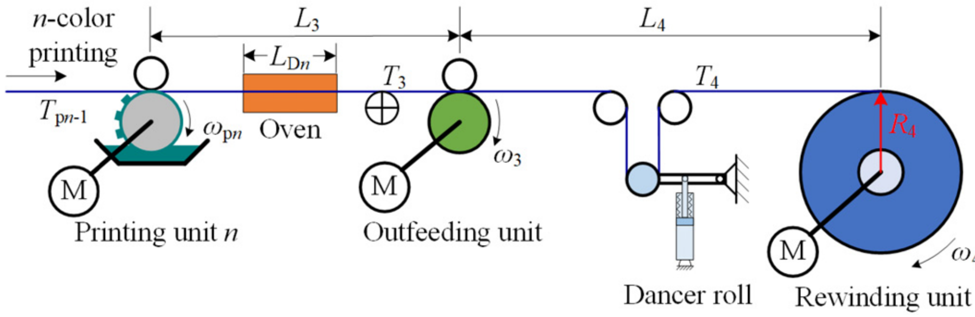

Figure 8. Structure of the rewinding subsystem.

respectively. In addition, R_{pn} and R_3 are the radius of the printing roll n and outfeeding roll.

The rewinding subsystem is similar to the unwinding subsystem. It can be regarded as the series of a two-roller system and a two-color printing system. In the same way, we ignore the influences of manufacturing errors, assembly errors and other factors, so L_3, L_{Dn}, R_3 and R_{pn} are fixed values. According to Eqs. (8) and (13), we can obtain the tension model of the rewinding subsystem as follows:

$$\begin{cases} \left[L_3 + L_{Dn}\left(\dfrac{E}{E_{Dn}} - 1\right)\right]\dfrac{\mathrm{d}T_3(t)}{\mathrm{d}t} \\ \quad = [AE - T_3(t)]R_3\omega_3(t) \\ \qquad - [AE - T_{pn}(t)]R_{pn}\omega_{pn}(t) \\ L_4(t)\dfrac{\mathrm{d}T_4(t)}{\mathrm{d}t} = [AE - T_4(t)]R_4(t)\omega_4(t) \\ \qquad\qquad - [AE - T_3(t)]R_3\omega_3(t) \\ \qquad\qquad + [AE - T_4(t)]\dfrac{\mathrm{d}L_4(t)}{\mathrm{d}t}. \end{cases} \tag{21}$$

The structure of the dancer roll installed in the rewinding unit is the same as that installed in the unwinding unit, so combining with Eqs. (16) and (17), the auxiliary equation of the tension model of the unwinding subsystem can be obtain as follows:

$$\begin{cases} L_4(t) = L_{u4} + \sqrt{L_{A2}^2 - [R_4(t) - r]^2} - 2\,\mathrm{d}_D\theta_r(t) \\ T_4(t) = -\dfrac{1}{2d_D}\left[J_D\dfrac{\mathrm{d}^2\theta_r(t)}{\mathrm{d}t^2} + B\dfrac{\mathrm{d}\theta_r(t)}{\mathrm{d}t} - F_r(t)d_K\right] \\ F_r(t) = P_r(t)A_C - K\theta_r(t)d_K. \end{cases} \tag{22}$$

Where L_{A2} is the center distance between the rewinding roll and the second guide roller of the dancer roll.

3.5 *Tension Model of the Global Tension System*

As shown in Fig. 1, the roll-to-roll n-color gravure printing machine can be regarded as the series of the unwinding subsystem, n-color printing subsystem and rewinding subsystem. Therefore, according to Eqs. (18), (20) and (21), the coupling mechanism model of the global tension system in the roll-to-roll n-color gravure printing machine can be obtained as follows:

$$\begin{cases} L_1(t)\dfrac{\mathrm{d}T_1(t)}{\mathrm{d}t} = [AE - T_1(t)]R_2\omega_2(t) \\ \qquad\qquad - [AE - T_u]R_1(t)\omega_1(t) \\ \qquad\qquad + [AE - T_1(t)]\dfrac{\mathrm{d}L_1(t)}{\mathrm{d}t} \\ L_2\dfrac{\mathrm{d}T_2(t)}{\mathrm{d}t} = [AE - T_2(t)]R_{p1}\omega_{p1}(t) \\ \qquad\qquad - [AE - T_1(t)]R_2(t)\omega_2(t) \\ \left[L_{p1} + L_{D1}\left(\dfrac{E}{E_{D1}} - 1\right)\right]\dfrac{\mathrm{d}T_{p1}(t)}{\mathrm{d}t} \\ \quad = [AE - T_{p1}(t)]R_{p2}\omega_{p2}(t) \\ \qquad - [AE - T_2(t)]R_{p1}\omega_{p1}(t) \\ \vdots \\ \left[L_{p(n-1)} + L_{D(n-1)}\left[\dfrac{E}{E_{D(n-1)}} - 1\right]\right]\dfrac{\mathrm{d}T_{p(n-1)}(t)}{\mathrm{d}t} \\ \quad = [AE - T_{p(n-1)}(t)]R_{pn}\omega_{pn}(t) \\ \qquad - [AE - T_{p(n-2)}(t)]R_{p(n-1)}\omega_{p(n-1)}(t) \\ \left[L_3 + L_{D_n}\left(\dfrac{E}{E_{D_n}} - 1\right)\right]\dfrac{\mathrm{d}T_3(t)}{\mathrm{d}t} \\ \quad = [AE - T_3(t)]R_3\omega_3(t) \\ \qquad - [AE - T_{pn}(t)]R_{pn}\omega_{pn}(t) \\ L_4(t)\dfrac{\mathrm{d}T_4(t)}{\mathrm{d}t} = [AE - T_4(t)]R_4(t)\omega_4(t) \\ \qquad\qquad - [AE - T_3(t)]R_3\omega_3(t) \\ \qquad\qquad + [AE - T_4(t)]\dfrac{\mathrm{d}L_4(t)}{\mathrm{d}t}. \end{cases} \tag{23}$$

Formula (19) and (22) are the auxiliary equations of the coupling model of the global tension system.

In the global tension system, the inputs are the angular velocities of functional units, and the outputs are the substrate tensions of tension sections. It can be seen from the Eq. (23) that the adjacent units of the global tension system are coupled together through the tension and velocity of the substrate. The global coupling mechanism model reflects the characteristics of coupling, nonlinearity and multi-disturbance in the tension system of the roll-to-roll n-color gravure printing machine.

Table I. Simulation parameters.

Parameters	Value	Unit
A	2.5×10^{-4}	m^2
E (20°C)	4.89×10^{9}	Pa
E_D (120°C)	0.62×10^{9}	Pa
E_D (150°C)	0.37×10^{9}	Pa
R_{1max}, R_{4max}	0.80	m
R_{1min}, R_{4min}	0.09	m
R_b	0.20	m
R_p	0.20	m
L_a	4.00	m
L_b	4.60	m
L_D	2.00	m
L_p	7.10	m
A_C	2.73×10^{-3}	m^2
d_D	0.35	m
d_K	0.15	m
K	559.00	N/m
B	0.01	N · m/(rad/s)
J_D	0.02	kg · m^2

4. SIMULATION AND ANALYSIS

To investigate the correctness of the established models, numerical simulations are carried out by using MATLAB 2019a in Windows 10 operating system environment. The simulation parameters used are the actual structure parameters of a model FR400 four-color gravure printing machine made by Shaanxi Beiren Printing Machinery Co., Ltd., and the relationships between the parameters are:

$$\begin{cases} R_2 = R_3 = R_b \\ R_{p1} = R_{p2} = R_{p3} = R_{p4} = R_p \\ L_1 = L_4 = L_a \\ L_2 = L_3 = L_b \\ L_{p1} = L_{p2} = L_{p3} = L_p \\ L_{D1} = L_{D2} = L_{D3} = L_{D4} = L_D \end{cases} \tag{24}$$

The substrate material used in the simulation is PET (Polyethylene terephthalate) film. Regardless of the manufacturing errors of mechanical parts, the values of simulation parameters are shown in Table I. The simulation flow chart is shown in Figure 9. All simulations adopt a fixed-step size mode, and the fixed-step size is 10 ms.

4.1 *Simulation of the Two-Color Printing System*

The simulation of the two-color printing system is carried out in this part. The tension model used in the simulation is as follows:

$$\left[L_p + L_D\left(\frac{E}{E_D} - 1\right)\right]\frac{\mathrm{d}T_{p1}(t)}{\mathrm{d}t} = [AE - T_{p1}(t)]R_p\omega_{p2}(t) - [AE - T_2(t)]R_p\omega_{p1}(t). \tag{25}$$

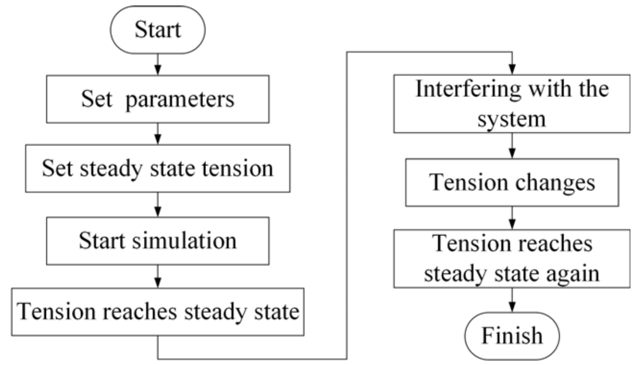

Figure 9. Simulation flow chart.

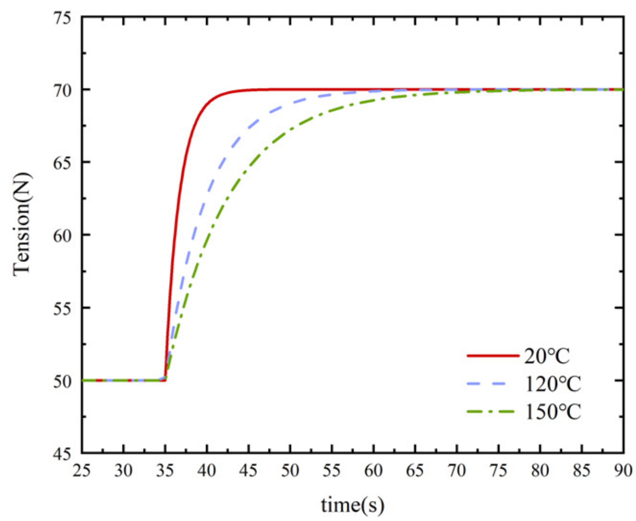

Figure 10. Response curves with a step change of T_2.

The ambient temperature is set at 20°C. Under initial conditions, the tension input of the two-color printing system is 50 N, and the steady state value of printing speed is 200 r/min. $T_2(t)$ has a step change from 50 N to 70 N at 35 s when oven temperature is 20°C, 120°C and 150°C. Tension response curves of the two-color printing system are shown in Figure 10. It can be seen from Fig. 10, the step change of $T_2(t)$ causes a step change of $T_{p1}(t)$, and the time that T_{p1} take to reach the steady state value is gradually increasing with an increase in the oven temperature. For example, when the temperature is equal to 120°C and 150°C, $T_{p1}(t)$ reaches 70 N at 37.5 s and 47 s, respectively.

Then, keeping $T_2(t)$ constant, $\omega_{p1}(t)$ decreases by 0.02 r/min, and the tension curves at different temperatures are shown in Figure 11. When $\omega_{p1}(t)$ generates a step signal, the time for $T_{p1}(t)$ to stabilize again at different temperatures is also different as shown in Fig. 11. When the oven temperature is 20°C, $T_{p1}(t)$ reaches stability again after 10.25 s. When the oven temperature is 120°C, $T_{p1}(t)$ reaches a stable state again after 32.5 s. When the oven temperature is 150°C, $T_{p1}(t)$ reaches a stable state again after 46.3 s.

Therefore, the transient response time of the two-color printing system becomes longer with the increase of the oven

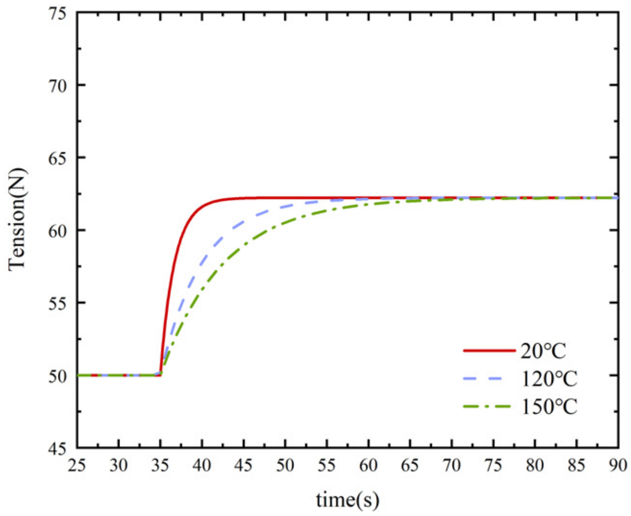

Figure 11. Response curves with a step change of ω_{p1}.

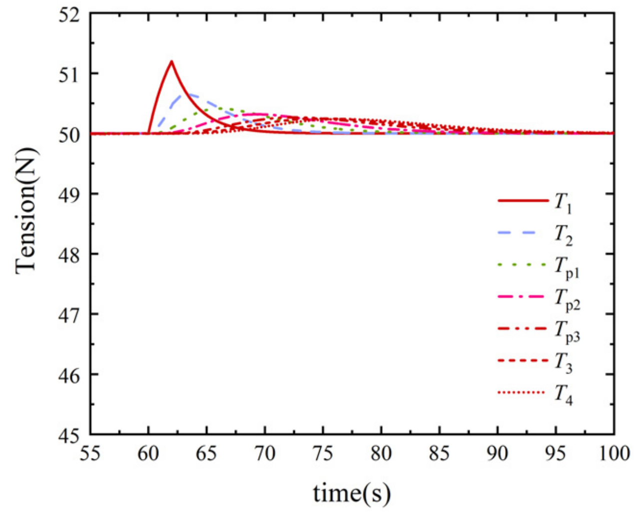

(a) Simulation curves at 100r/min

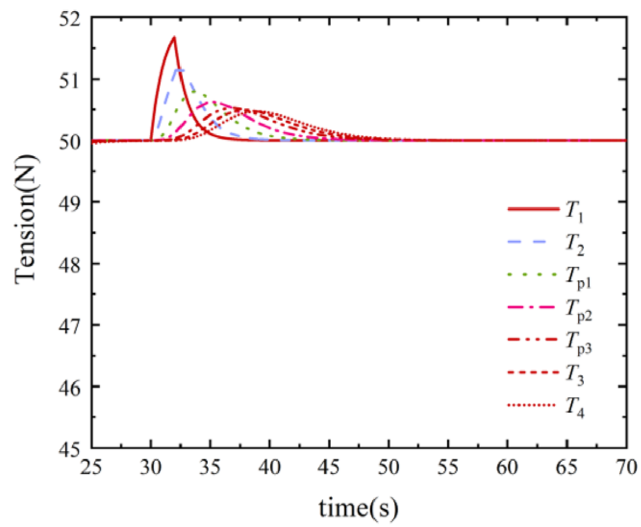

(b) Simulation curves at 200r/min

Figure 12. Simulation results of changing T_u.

temperature. It can be shown from the simulation that the tension model of the two-color printing system established in this paper can reflect the characteristics of the tension system and also reveal the influences of temperature on the tension system.

4.2 *Simulation of the Global Coupling System*

To analyze the global tension coupling model of the roll-to-roll gravure printing machine, a tension system simulation model of a four-color gravure printing machine is established in MATLAB. Combining with Eqs. (23) and (24), the simulation model used is as follows:

$$
\begin{cases}
L_a \dfrac{dT_1(t)}{dt} = [AE - T_1(t)]R_b\omega_2(t) \\
\qquad - [AE - T_u]R_1\omega_1(t) \\
L_b \dfrac{dT_2(t)}{dt} = [AE - T_2(t)]R_p\omega_{p1}(t) \\
\qquad - [AE - T_1(t)]R_b\omega_2(t) \\
\left[L_p + L_D\left(\dfrac{E}{E_D} - 1\right)\right]\dfrac{dT_{p1}(t)}{dt} \\
\quad = [AE - T_{p1}(t)]R_p\omega_{p2}(t) \\
\qquad - [AE - T_2(t)]R_p\omega_{p1}(t) \\
\left[L_p + L_D\left(\dfrac{E}{E_D} - 1\right)\right]\dfrac{dT_{p2}(t)}{dt} \\
\quad = [AE - T_{p2}(t)]R_p\omega_{p3}(t) - [AE - T_{p1}(t)]R_p\omega_{p2}(t) \\
\left[L_p + L_D\left(\dfrac{E}{E_D} - 1\right)\right]\dfrac{dT_{p3}(t)}{dt} \\
\quad = [AE - T_{p3}(t)]R_p\omega_{p4}(t) - [AE - T_{p2}(t)]R_p\omega_{p3}(t) \\
\left[L_b + L_D\left(\dfrac{E}{E_D} - 1\right)\right]\dfrac{dT_3(t)}{dt} \\
\quad = [AE - T_3(t)]R_3\omega_3(t) - [AE - T_{p4}(t)]R_p\omega_{p4}(t) \\
L_a \dfrac{dT_4(t)}{dt} = [AE - T_4(t)]R_4\omega_4(t) \\
\qquad - [AE - T_3(t)]R_b\omega_3(t).
\end{cases} \tag{26}
$$

4.2.1 *Simulation Under a Step Disturbance of T_u*

When the synchronous velocity of the system is 100 r/min and 200 r/min, and the steady-state tension is 50 N, T_u is made to generate step disturbance of 2 N size and 2 s duration. The simulation results are shown in Figure 12.

As shown in Fig. 12, when T_u produces a step interference, the tensions of the global tension system are affected by the tension interference and produce fluctuations. The tension interference of T_u has different degrees of influences on the tensions of the subsequent sections, and the magnitude of the influences decreases gradually. By comparing Fig. 11(a) and (b), it can be seen that the adjustment time for tensions to reach the stable state is shorter when the synchronization velocity is higher. When the synchronization velocity is 100 r/min, the tension of each section is disturbed and reaches the stable state again after 46 s. When the synchronization velocity is 200 r/min,

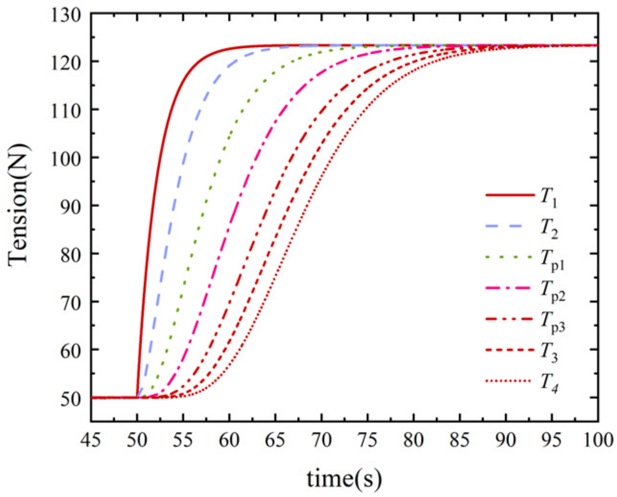

(a) Simulation curves at 100r/min

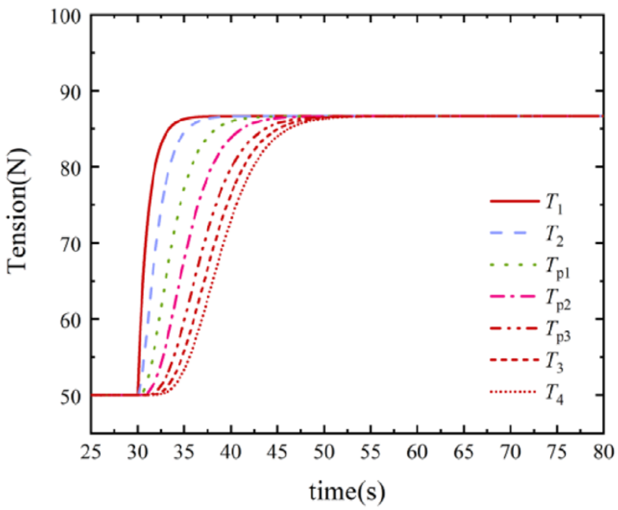

(b) Simulation curves at 200r/min

Figure 13. Simulation results of changing $\omega_1(t)$.

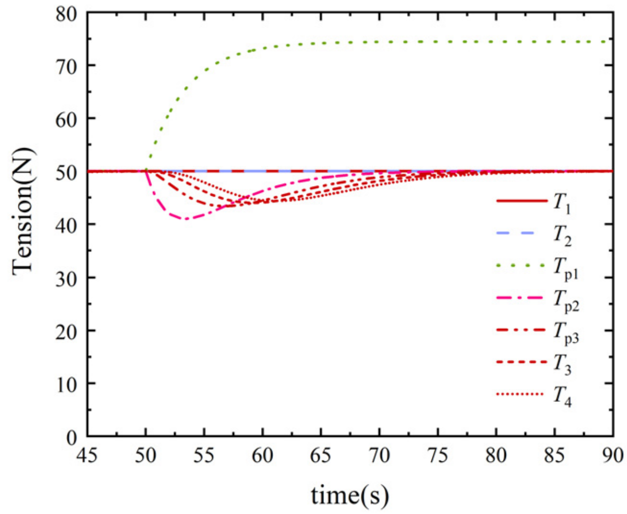

(a) Simulation curves at 100r/min

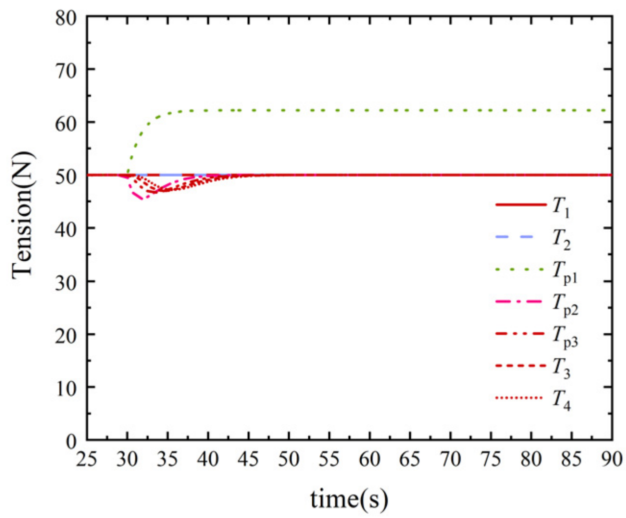

(b) Simulation curves at 200r/min

Figure 14. Simulation results of changing $\omega_{p2}(t)$.

the tension of each section is disturbed and reaches the stable state again after 29.21 s. The simulation results illustrate that the substrate tension has the characteristics of transmission.

4.2.2 *Simulation Under a Step Disturbance of $\omega_1(t)$*

The $\omega_1(t)$ is decreased by 0.02 r/min, when the synchronous velocity of the system is 100 r/min and 200 r/min, and the steady-state tension is 50 N. Figure 13 illustrates simulation results.

It can be seen from Fig. 13 that when $\omega_1(t)$ is changed, $T_1(t)$ changes first, and then the tensions of the subsequent sections are influenced successively. After a period of change, the tensions of all sections finally reach stable a state again. In addition, by comparing the two simulation results of the Fig. 13(a) and (b), it can be seen that under the same disturbance of $\omega_1(t)$, the time for the tension of each section to reach the steady-state value decreases with the increase of synchronization velocity. When the synchronization velocity is 100 r/min, the tension of each section reaches the stable state again after 47.67 s. When the synchronization velocity is 200 r/min, the tension of each section reaches the stable state again after 35.54 s. The simulation results show that the tension system of roll-to-roll gravure printing machines has the characteristics of coupling and the transferability of tension.

4.2.3 *Simulation Under a Step Disturbance of $\omega_{p2}(t)$*

When the synchronous velocity of the system is 100 r/min and 200 r/min, and the steady-state tension is 50 N, $\omega_{p2}(t)$ is increased by 0.02 r/min. The simulation results are illustrated in Figure 14.

Fig. 14 indicates that when $\omega_{p2}(t)$ is changed, $T_{p1}(t)$ changes first, and it affects the tension output of all subsequent sections, but not on $T_1(t)$ and $T_2(t)$. When the synchronization velocity is 100 r/min, $T_{p1}(t)$ reaches the stable state again after 33.23 s, and the new steady state value of $T_{p1}(t)$ is 74.45 N. When the synchronization velocity is 200 r/min, $T_{p1}(t)$ reaches the stable state again after 19.66 s, and the new steady state value of $T_{p1}(t)$ is 62.22 N. The simulation results show that the tension of each section propagates backward in roll-to-roll gravure printing machines, that is to say, the change of the tension from the current section will not affect the tension output of the previous section, but will affect the tension output of all subsequent sections.

5. CONCLUSION

In this paper, the coupling mechanism model of global tension system is derived and analyzed in detail for the roll-to-roll gravure printing machines. Considering the effect of drying temperature, we derive the tension model of the two-color printing system which reveals the multi-source mechanism of substrate tension variation. According to the tension models of the unwinding subsystem, n-color printing subsystem and rewinding subsystem, we establish the coupling mechanism model of the global tension system which reflects the characteristics of coupling, nonlinearity and multi-disturbance in the tension system. The research results of this paper provide guidance and reference for the study of tension systems in various roll-to-roll printing equipment, and also have important value for proposing a suitable tension control method for the characteristics of tension systems in roll-to-roll gravure printing machines.

The tension models are established under the conditions of several basic assumptions, which are some differences between the actual tension systems of the roll-to-roll gravure printing machine. Therefore, in the follow-up research, we would be conducting a more detailed and comprehensive verification of the tension models established in this paper through experiments.

ACKNOWLEDGMENT

This project is supported by the national key research and development program of China (Grant No. 2019YFB1707200), the key research and development program of Shaanxi Province (Grant No. 2020ZDLGY14-06), the technology innovation leading program of Shaanxi Province (Grant No. 2020QFY03-03 and 2020QFY03-08) and the key research projects of Henan Province (Grant No. 212102210356).

REFERENCES

[1] C. Jiang, H. Wang, L. Hou, and L. Jiang, "Sliding mode compensation control for diaphragm tension in unwinding process of lithium battery diaphragm slitting machine," IEEE Access **8**, 21302–21313 (2020).

[2] S. Liu, X. Mei, F. Kong, and K. He, "A decoupling control algorithm for unwinding tension system based on active disturbance rejection control," Math. Probl. Eng. **18**, 2013 (2013).

[3] S. W. Jeon, C. Kim, and C. H. Kim, "Fast stabilization of web tension in drying process of roll-to-roll printing equipment for printed electronics," J. Mech. Sci. Technol. **29**, 5069–5074 (2015).

[4] R. V. Dwivedula and P. R. Pagilla, "Effect of backlash on web tension in roll-to-roll manufacturing systems: Mathematical model, mitigation method and experimental evaluation," *Int'l. Conf. on Control Applications* (IEEE, Piscataway, NJ, 2013), pp. 1087–1092.

[5] J. Jeong, A. N. Gafurov, P. Park, I. Kim, H. C. Kim, D. Kang, and T. M. Lee, "Tension modeling and precise tension control of roll-to-roll system for flexible electronics," Flex. Print Electron. **6**, 015005 (2021).

[6] K. Seki, T. Kikuchi, and M. Iwasaki, "Tension controller design considering periodic disturbance suppression in roll-to-roll web handling systems," IEEJ J. Ind. Appl. **9**, 36–42 (2020).

[7] H. Huang, J. Xu, K. Sun, L. Deng, and C. Huang, "Design and analysis of tension control system for transformer insulation layer winding," IEEE Access **8**, 95068–95081 (2020).

[8] Z. Gu, S. Zeng, K. Zhao, and C. Song, "Fully-digital tension control system with PID algorithm for winding ultra-fine enameled wires," Mater. Sci. Eng. **892**, 012064 (2020).

[9] K. He, G. Zhou, T. Xiong, and S. Wei, "Periodic tension disturbance attenuation using plug-in repetitive controller in web unwinding process," *Chinese Automation Congress* (IEEE, Piscataway, NJ, 2020), pp. 7467–7472.

[10] A. Seshadri and P. R. Pagilla, "Modeling and analysis of a rotating turret winder in roll-to-roll manufacturing systems," *American Control Conf.* (IEEE, Piscataway, NJ, 2018), pp. 6667–6672.

[11] S. Wang, F. He, and Q. Wang, "Integral separation fuzzy PID control for winding tension system," *PChinese Control and Decision Conf.* (IEEE, Piscataway, NJ, 2019), pp. 4083–4088.

[12] J. Chen, H. Hou, and T. Yang, "Robust decentralized $H\infty$ control for a multi-motor web-winding system," IEEE Access **7**, 41241–41249 (2019).

[13] B. Kuznetsov, T. Nikitina, I. Bovdui, and B. Kobilyanskiy, "Robust anisotropic control by cable winding machine," *Modern Electrical and Energy Systems* (IEEE, Piscataway, NJ, 2019), pp. 38–41.

[14] E. Torres and P. R. Pagilla, "A governing equation for moving web temperature heated by radiative panels," *American Control Conf.* (IEEE, Piscataway, NJ, 2016), 858–863.

[15] E. Torres and P. R. Pagilla, "Temperature distribution in moving webs heated by radiation panels: Model development and experimental validation," J. Dyn. Syst. Meas. Control **139**, 051003 (2017).

[16] K. He, T. Tao, and S. Liu, "Analysis for effects of drying temperature on web tension in gravure printing machine," J. Xi'an Jiaotong University **52**, 150–156 (2018).

[17] C. Lee, H. Kang, and K. Shin, "A study on tension behavior considering thermal effects in roll-to-roll E-printing," J. Mech. Sci. Technol. **24**, 1097–1103 (2010).